Physics of Fluids LETTER scitation.org/journal/phf

Minimal error partially resolving simulation methods for turbulent flows: A dynamic machine learning approach

Cite as: Phys. Fluids **34**, 051705 (2022); doi: 10.1063/5.0095592
Submitted: 11 April 2022 · Accepted: 5 May 2022 ·
Published Online: 20 May 2022

Stefan Heinz[a]

AFFILIATIONS

Mathematics and Statistics Department, University of Wyoming, 1000 East University Avenue, Laramie, Wyoming 82071, USA

[a]Author to whom correspondence should be addressed: heinz@uwyo.edu

ABSTRACT

A significant extension of previously introduced continuous eddy simulation methods is presented by introducing minimal error partially and fully resolving simulation methods for turbulent flows. This approach represents a machine learning strategy for the hybridization of modeling-focused and resolution-focused simulation methods. It can be applied to well-known equation structures (Spalart–Allmaras type equations, usually applied two-equation models), and it can be used for different hybridization types and in different computational versions. Physically, minimal error methods implement a mode interplay, which ensures that the resolution imposed by a model equals the actual flow resolution. Differently formulated simulation methods reveal two typical errors, and they cannot be expected to provide reliable predictions under conditions where validation data are unavailable. These problems can be avoided by minimal error formulations of model structures considered.

The development of simulation methods for turbulent flows faces known problems.[1,2] Reynolds-averaged Navier–Stokes (RANS) methods focusing on flow modeling cannot reliably handle complex flows involving flow separation, as very often seen in applications. Large eddy simulation (LES) methods focusing on flow resolution are usually constrained by their resolution requirements, especially for wall-bounded turbulent flows at high Reynolds number (*Re*). Hybrid RANS–LES methods[2–4] were developed to overcome the inapplicability of LES and unreliability of RANS. However, there is now a large variety of such hybrid methods, traditionally applied methods like wall-modeled LES (WMLES)[5–11] and detached eddy simulation (DES),[4,12–16] and other methods such as scale adaptive simulation (SAS) methods,[4,17,18] lattice Boltzmann (LB) methods,[19–21] Reynolds-stress-constrained LES (RSC-LES),[22] unified RANS–LES,[23–31] partially averaged Navier–Stokes (PANS),[32–34] partially integrated transport modeling (PITM) methods,[35,36] and continuous eddy simulation (CES) methods.[2,37–43] There have been recent attempts to use machine learning (ML) methods [seen here as computer-aided methods that apply sample data to (iteratively) improve analyses, models, or simulations, often by minimizing errors] to address the inability of RANS to deal with separated flow.[44] It may be expected that further developments of hybrid RANS–LES will take place in future decades as long as there is no convincing guideline about which out of the many available hybrid RANS–LES have to be preferred.

It is impossible to derive general conclusions via applications of many hybrid methods to many turbulent flows; that is, it needs theoretical guideline to address this issue. Several hybrid RANS–LES were presented as having theoretical support,[2] leading to the question of which theoretical concept should be preferred. For example, CES methods introduced recently are implied by theory.[2,37–42] For PANS and PITM structures, it was shown how information about the actual flow resolution can be implemented in these models (using an approximation, the neglect of substantial derivatives). The methods were demonstrated to work very well in applications.[38,43] It was also shown that eddy viscosity model (EVM) PANS and PITM structures can be extended to Reynolds-stress models (RSM) and probability density function (PDF) methods applicable to both turbulent velocity and scalar fields.[39] The question left unaddressed is whether the CES implementation of resolution information, which differs from other hybrid RANS–LES, has to be preferred.

The purpose of this paper is to introduce minimal error hybrid RANS–LES models to provide a basis for the evaluation of model concepts. This will be done by considering usually applied turbulence models and hybridization methods including DES and WMLES,

which were not analyzed before in this context. It matters to clarify assumptions applied. In an analysis option $\mathcal{O}_1$, we apply two assumptions. Assumption $\mathcal{A}_1$ is that RANS-type equations can be used to also cover the LES regime. This assumption (which is applied by almost all hybrid RANS–LES) has strong theoretical support[2] including the fact that it is a requirement for the design of a realizable turbulence model.[25] The analysis here provides additional evidence [see the discussion of Eq. (2)]. First, the RANS-type equations considered are structurally consistent with regularly applied LES. Second, among all equations that can be considered for RANS and LES, the equation error can be minimized by considering the same equations to perform both RANS and LES. The attempt to relax assumption $\mathcal{A}_1$ has a significant price, it produces a variety of problems that need empirical solutions, and it does not enable minimal error formulations.[45] Assumption $\mathcal{A}_2$ is that the energy partition ($\delta k/k$ and $\delta\epsilon/\epsilon$, see below) does not change in space and time. This assumption is not a restriction but a desired stability requirement, and it ensures that physically equivalent flow regions are equally resolved without significant oscillations of $\delta k/k$ and $\delta\epsilon/\epsilon$.[37–40] As alternative to $\mathcal{O}_1$, an option $\mathcal{O}_2$ will be considered below, which represents a possible but not required simplification of option $\mathcal{O}_1$.

The analysis basis is given by the incompressible continuity equation $\partial\tilde{U}_i/\partial x_i = 0$ and the momentum equation

$$\frac{D\tilde{U}_i}{Dt} = -\frac{1}{\rho}\frac{\partial\tilde{p}}{\partial x_i} + \frac{\partial(2\nu\tilde{S}_{ij})}{\partial x_j} - \frac{\partial\tau_{ij}}{\partial x_j}. \tag{1}$$

The tilde refers to space-averaged variables, and $D/Dt = \partial/\partial t + \tilde{U}_j\partial/\partial x_j$ is the filtered Lagrangian time derivative (t is time, and x_j refers to components of the position vector). $\tilde{U}_i$ refers to components of the velocity vector, $\tilde{p}$ is the pressure, ρ is the constant fluid density, ν is the constant kinematic viscosity, and $\tilde{S}_{ij} = (\partial\tilde{U}_i/\partial x_j + \partial\tilde{U}_j/\partial x_i)/2$ is the rate-of-strain tensor. The sum convention is used throughout this paper. The modeled stress tensor τ_{ij} on the right-hand side (RHS) of Eq. (1) is modeled by an EVM, $\tau_{ij} = 2k\delta_{ij}/3 - 2\nu_t\tilde{S}_{ij}$. Here, δ_{ij} is the Kronecker symbol, and $\nu_t = C_\mu k^2/\epsilon = C_\mu k/\omega$ is the modeled viscosity, which involves the model parameter C_μ, the modeled kinetic energy k, dissipation rate ϵ, and turbulence frequency ω.[29,30] The reason why emphasis is placed on an EVM is the simplicity of equations: it was shown recently[39] that the extension to corresponding RSM and PDF methods is straightforward.

To illustrate the approach, let us consider first $k-\epsilon$ model-based KES and KEK equations given in Table I: KE refers to the $k-\epsilon$ model, and KES and KEK refer to the hybridization of the scale equation or k equation, respectively. The setup of equations considered covers hybrid formulations used in DES, PANS, PITM, and CES methods. $P = \nu_t S^2$ is the turbulence production involving the strain rate $S = (2\tilde{S}_{mn}\tilde{S}_{nm})^{1/2}$. We have $C_{\epsilon_1} = 1.44$ and $\sigma_\epsilon = 1.3$. In RANS, $\alpha = C_{\epsilon_2}/C_{\epsilon_1}$ where $C_{\epsilon_2} = 1.92$ implies $\alpha = 1.33$. The hybridization of KES (KEK) equations is addressed by replacing α by an unknown α^* (by replacing ϵ by $\psi_\alpha\epsilon$, where ψ_α is an unknown). Both KES and KEK equations can be hybridized in analysis options $\mathcal{O}_1$ or $\mathcal{O}_2$. The difference of versions is that contributions due to Dk/Dt and $D\epsilon/Dt$ are considered in option $\mathcal{O}_1$ but neglected in option $\mathcal{O}_2$. The advantage of option $\mathcal{O}_2$ is that these equations do not explicitly involve resolved contributions via the total modeled viscosity $\nu_{t,tot}$.[2] The latter need to be considered in option $\mathcal{O}_1$ equations to compensate the inclusion of Dk/Dt and $D\epsilon/Dt$.[40]

Minimal error methods of equations considered in Table I can be derived in the following way. The analysis of KES and KEK equations is equivalent: it simply needs to make use of $\alpha^* = 1 + \alpha - \psi_\alpha$. We introduce a model error λ as residual of the ϵ equation. P is replaced according to the k equation in this error definition. We apply assumption $\mathcal{A}_2$, see the third paragraph. The first variations (denoted by δ) of normalized errors λ/ϵ and λ/k^2 are obtained, where relations for δD_k, δD_ϵ, $\delta(Dk/Dt)$, and $\delta(D\epsilon/Dt$ given in the bracket terms of Table I are applied. The expressions obtained for error variations make use of the error definition to replace D_ϵ. An extremal error is given for a vanishing first variation, $\delta\alpha_1^* = (\alpha_1^* - 1)\delta\tau/\tau$ (option $\mathcal{O}_1$) and $\delta\alpha_2^* = (\alpha_2^* - 1)\delta L^2/L^2$ (option $\mathcal{O}_2$). Here, $\tau = k/\epsilon = \omega^{-1}$ is the dissipation time scale and $L = k^{1.5}/\epsilon$ refers to the modeled length scale of turbulence. The integration of zero first variation relations from a complete modeling state to a state of partial modeling implies $\alpha_1^* = 1 + \tau_+(\alpha - 1)$ and $\alpha_2^* = 1 + L_+^2(\alpha - 1)$.[37] Here, $\tau_+ = \tau/\tau_{tot}$ and $L_+ = L/L_{tot}$ refer to the modeled to total time scale and length scale ratios (see the Appendix). We note that α_1^* and α_2^* recover CES results.[37,40] For all models considered in this paper, we find a zero

TABLE I. Minimal error $k-\epsilon$ models: both KES and KEK hybridizations are considered in analysis options $\mathcal{O}_1$, $\mathcal{O}_2$ depending on ν_t^*. Model errors λ, first variations, and resulting mode controls α^* are provided. Variations applied are given in brackets.

$$\frac{Dk}{Dt} = P - \epsilon + D_k, \quad \frac{D\epsilon}{Dt} = C_{\epsilon_1}\frac{\epsilon^2}{k}\left(\frac{P}{\epsilon} - \alpha^*\right) + D_\epsilon, \quad D_k = \frac{\partial}{\partial x_j}\nu_t^*\frac{\partial k}{\partial x_j}, \quad D_\epsilon = \frac{\partial}{\partial x_j}\frac{\nu_t^*}{\sigma_\epsilon}\frac{\partial\epsilon}{\partial x_j}\ \text{(KES)}$$

$$\frac{Dk}{Dt} = P - \psi_\alpha\epsilon + D_k, \quad \frac{D\epsilon}{Dt} = C_{\epsilon_1}\frac{\epsilon^2}{k}\left(\frac{P}{\epsilon} - \alpha\right) + D_\epsilon, \quad \alpha^* = 1 + \alpha - \psi_\alpha \qquad \text{(KEK)}$$

• Analysis option $\mathcal{O}_1$ (with $Dk/Dt, D\epsilon/Dt$, $\nu_t^* = \nu_{t,tot}$): $\left[\frac{\delta(Dk/Dt)}{Dk/Dt} = \frac{\delta D_k}{D_k} = \frac{\delta k}{k}, \quad \frac{\delta(D\epsilon/Dt)}{D\epsilon/Dt} = \frac{\delta D_\epsilon}{D_\epsilon} = \frac{\delta\epsilon}{\epsilon}\right]$

$$\lambda_1 = C_{\epsilon_1}\frac{\epsilon^2}{k}\left(\frac{P}{\epsilon} - \alpha_1^*\right) + D_\epsilon - \frac{D\epsilon}{Dt}, \quad \delta\left(\frac{\lambda_1}{\epsilon}\right) = \frac{C_{\epsilon_1}}{\tau}(\alpha_1^* - 1)\left[\frac{\delta\tau}{\tau} - \frac{\delta\alpha_1^*}{\alpha_1^* - 1}\right], \quad \int_\alpha^{\alpha_1^*}\frac{dx}{x-1} = \int_{\tau_{tot}}^{\tau}\frac{dy}{y}, \quad \frac{\alpha_1^* - 1}{\alpha - 1} = \tau_+$$

• Analysis option $\mathcal{O}_2$ (without $Dk/Dt, D\epsilon/Dt$, $\nu_t^* = \nu_t$): $[\delta D_k/D_k = 3\delta k/k - \delta\epsilon/\epsilon, \quad \delta D_\epsilon/D_\epsilon = 2\delta k/k]$

$$\lambda_2 = C_{\epsilon_1}\frac{\epsilon^2}{k}\left(\frac{P}{\epsilon} - \alpha_2^*\right) + D_\epsilon, \quad \delta\left(\frac{\lambda_2}{k^2}\right) = \frac{C_{\epsilon_1}}{L^2}(\alpha_2^* - 1)\left[\frac{\delta L^2}{L^2} - \frac{\delta\alpha_2^*}{\alpha_2^* - 1}\right], \quad \int_\alpha^{\alpha_2^*}\frac{dx}{x-1} = \int_{L_{tot}^2}^{L^2}\frac{dy}{y}, \quad \frac{\alpha_2^* - 1}{\alpha - 1} = L_+^2$$

TABLE II. Minimal error $k-\omega$ models: both KOS and KOK hybridizations are considered in analysis options $\mathcal{O}_1$, $\mathcal{O}_2$ depending on ν_t^*. Model errors λ, first variations, and resulting mode controls β^* are provided. Variations applied are given in brackets.

$$\frac{Dk}{Dt}=P-\epsilon+D_k,\quad \frac{D\omega}{Dt}=C_{\omega_1}\omega^2\left(\frac{P}{\epsilon}-\beta^*\right)+D_\omega,\quad D_k=\frac{\partial}{\partial x_j}\nu_t^*\frac{\partial k}{\partial x_j},\quad D_\omega=\frac{\partial}{\partial x_j}\frac{\nu_t^*}{\sigma_\omega}\frac{\partial\omega}{\partial x_j}\ \text{(KOS)}$$

$$\frac{Dk}{Dt}=P-\psi_\beta\epsilon+D_k,\quad \frac{D\omega}{Dt}=C_{\omega_1}\omega^2\left(\frac{P}{\epsilon}-\beta\right)+D_\omega,\quad \beta^*=1+\beta-\psi_\beta\qquad\text{(KOK)}$$

• Analysis option $\mathcal{O}_1$ (with $Dk/Dt, D\omega/Dt$, $\nu_t^*=\nu_{t,tot}$): $\left[\frac{\delta(Dk/Dt)}{Dk/Dt}=\frac{\delta D_k}{D_k}=\frac{\delta k}{k},\quad \frac{\delta(D\omega/Dt)}{D\omega/Dt}=\frac{\delta D_\omega}{D_\omega}=\frac{\delta\omega}{\omega}\right]$

$$\lambda_1=C_{\omega_1}\omega^2\left(\frac{P}{\epsilon}-\beta_1^*\right)+D_\omega-\frac{D\omega}{Dt},\quad \delta\left(\frac{\lambda_1}{\omega}\right)=\frac{C_{\omega_1}}{\tau}(\beta_1^*-1)\left[\frac{\delta\tau}{\tau}-\frac{\delta\beta_1^*}{\beta_1^*-1}\right],\quad \int_\beta^{\beta_1^*}\frac{dx}{x-1}=\int_{\tau_{tot}}^{\tau}\frac{dy}{y},\quad \frac{\beta_1^*-1}{\beta-1}=\tau_+$$

• Analysis option $\mathcal{O}_2$ (without $Dk/Dt, D\omega/Dt$, $\nu_t^*=\nu_t$): $\left[\delta D_k/D_k=3\delta k/k-\delta\epsilon/\epsilon,\quad \delta D_\omega/D_\omega=\delta k/k\right]$

$$\lambda_2=C_{\omega_1}\omega^2\left(\frac{P}{\epsilon}-\beta_2^*\right)+D_\omega,\quad \delta\left(\frac{\lambda_2}{k}\right)=\frac{C_{\omega_1}}{L^2}(\beta_2^*-1)\left[\frac{\delta L^2}{L^2}-\frac{\delta\beta_2^*}{\beta_2^*-1}\right],\quad \int_\beta^{\beta_2^*}\frac{dx}{x-1}=\int_{L_{tot}^2}^{L^2}\frac{dy}{y},\quad \frac{\beta_2^*-1}{\beta-1}=L_+^2$$

second variation, and we need to ask whether α_1^* and α_2^* provide a minimum or maximum error. The results are equal to variational results obtained by considering $\lambda=0$; that is, the analysis presented implies minimal error models.

Corresponding results can be also obtained on the basis of $k-\omega$ models, $\omega=\tau^{-1}$ is the turbulence frequency (see Table II). Here, KO refers to the use of $k-\omega$ models, and KOS and KOK refer to hybridizations of the scale or k equation, respectively. The model parameters involved are given by $C_{\omega_1}=0.49$ and $\sigma_\omega=1.8$. In RANS, $\beta=C_{\omega_2}/(C_kC_{\omega_1})$ where $C_{\omega_2}=0.072$ and $C_k=0.09$ imply $\beta=1.63$. A cross-diffusion term $D_{\omega c}=C_\omega k^{-1}(\nu+\nu_t)[\partial k/\partial x_j][\partial\omega/\partial x_j]$ is often added to the ω equation, which acts like a damping function. It is disregarded for the following analysis. The hybridization of the KOS (KOK) equations is accomplished by replacing β by an unknown β^* (by replacing ϵ by $\psi_\beta\epsilon$, where ψ_β is an unknown). Minimal error methods of equations considered in Table II can be derived in the same way as regarding the corresponding $k-\epsilon$ methods. The analysis of KOS and KOK equations is equivalent if $\beta^*=1+\beta-\psi_\beta$ is applied. Minimal error conditions follow from setting the first variations equal to zero. The integration of these minimal error conditions provides $\beta_1^*=1+\tau_+(\beta-1)$ and $\beta_2^*=1+L_+^2(\beta-1)$ for analysis options $\mathcal{O}_1$ and $\mathcal{O}_2$, respectively, which recover again corresponding CES results. Similar to the analysis of $k-\epsilon$ models, we applied here variational relations for diffusion coefficients and substantial derivatives given in the bracket terms of Table II.

The same approach can be applied to ν_t models by considering equations, which cover methods applied in DES and SAS approaches, see also Ref. 46. Related results are presented in Table III, and specific DES and SAS settings are given in Table IV. Production (c_p), dissipation (c_d), and turbulent diffusion (σ and c_{b2}) model parameters are defined in terms of usually applied parameters [the von Kármán constant κ applied differs slightly from the universal value $\kappa=0.4$

TABLE III. Minimal error DES–SAS type ν_t models in options $\mathcal{O}_1$, $\mathcal{O}_2$ depending on ν_t^*. Model errors λ, first variations, resulting mode controls γ^*, and variations applied are provided. Relations of γ and γ^* with D and D_*, and implications for D_* in options $\mathcal{O}_1$ and $\mathcal{O}_2$ (D_1^{*2} and D_2^{*2}) are given in the last row. Specific DES and SAS settings are provided in Table IV.

$$\frac{D\nu_t}{Dt}=c_pS\nu_t(1-\gamma^*)+D_\nu,\quad D_\nu=\frac{\partial}{\partial x_j}\frac{\nu_t^*}{\sigma}\frac{\partial\nu_t}{\partial x_j}+\frac{c_{b2}}{\sigma}\frac{\partial\nu_t^*}{\partial x_j}\frac{\partial\nu_t}{\partial x_j}\quad\text{(DES–SAS)}$$

• Analysis option $\mathcal{O}_1$ (with $D\nu_t/Dt$, $\nu_t^*=\nu_{t,tot}$): $\left[\frac{\delta(D\nu_t/Dt)}{D\nu_t/Dt}=\frac{\delta D_\nu}{D_\nu}=\frac{\delta\nu_t}{\nu_t}\right]$

$$\lambda_1=c_pS\nu_t(1-\gamma_1^*)+D_\nu-\frac{D\nu_t}{Dt},\quad \delta\left(\frac{\lambda_1}{\nu_t}\right)=c_pS(\gamma_1^*-1)\left[\frac{\delta S^{-1}}{S^{-1}}-\frac{\delta\gamma_1^*}{\gamma_1^*-1}\right],\quad \int_\gamma^{\gamma_1^*}\frac{dx}{x-1}=\int_{S_{tot}^{-1}}^{S^{-1}}\frac{dy}{y},\quad \frac{\gamma_1^*-1}{\gamma-1}=S_+^{-1}$$

• Analysis option $\mathcal{O}_2$ (without $D\nu_t/Dt$, $\nu_t^*=\nu_t$): $\left[\delta D_\nu/D_\nu=2\delta\nu_t/\nu_t\right]$

$$\lambda_2=c_pS\nu_t(1-\gamma_2^*)+D_\nu,\quad \delta\left(\frac{\lambda_2}{\nu_t^2}\right)=\frac{c_p}{\ell^2}(\gamma_2^*-1)\left[\frac{\delta\ell^2}{\ell^2}-\frac{\delta\gamma_2^*}{\gamma_2^*-1}\right],\quad \int_\gamma^{\gamma_2^*}\frac{dx}{x-1}=\int_{\ell_{tot}^2}^{\ell^2}\frac{dy}{y},\quad \frac{\gamma_2^*-1}{\gamma-1}=\ell_+^2$$

Length scale interpretation: $\gamma=\frac{c_d\,\ell_{tot}^2}{c_pD^2},\quad \gamma^*=\frac{c_d\,\ell^2}{c_pD^{*2}},\quad D_1^{*2}=\frac{\gamma\ell_+^2D^2}{1+S_+^{-1}(\gamma-1)},\quad D_2^{*2}=\frac{\gamma\ell_+^2D^2}{1+\ell_+^2(\gamma-1)}$

TABLE IV. DES and SAS settings related to Table III. The log-law consistency conditions read $c_d = c_p/\kappa^2 + (1+c_{b2})/\sigma$: for SAS, we obtain $\sigma C_\mu^{1/2}(\zeta_2 - \zeta_1 + C_\mu^{-3/4}\zeta_3) = \kappa^2$.

DES: $D = d/f_w^{1/2}$,
$c_p = c_{b1}, c_d = c_{w1} = c_{b1}/\kappa^2 + (1+c_{b2})/\sigma$
$(c_{b1}, c_{b2}, \sigma, \kappa) = (0.1355, 0.622, 2/3, 0.41)$
SAS: $D = \ell_{vK,tot}$, $a = C_\mu C_{\mu*}^{-1/2}$,
$c_p = a(\zeta_1 - \zeta_3 C_\mu^{1/4}/a^2), c_d = \zeta_2 a^2/(C_\mu^{1/2}\kappa^2)$,
$(\zeta_1, \zeta_2, \zeta_3, c_{b2}, \sigma, \kappa, C_\mu)$
$= (0.8, 1.47, 0.0288, 0, 2/3, 0.41, 0.09)$

(Refs. 47 and 48)]. Here, $a = \nu_t S/k = C_\mu C_{\mu^*}^{-1/2}$ is Bradshaw's constant (we introduced $S\tau = C_{\mu^*}^{-1/2}$), and it has a log-law value $a = C_\mu^{1/2}$. According to the model structure, we define a characteristic length scale by $\ell^2 = \nu_t/S$. Different definitions can be applied for the characteristic shear rate $S > 0$. For the following, there is no need to specify S. The fully modeled dissipation is denoted by γ, and γ^* refers to the hybridized non-dimensional dissipation. A conceptual difference to $k-\epsilon$ and $k-\omega$ models is the specification of the structure of $\gamma = c_d \ell_{tot}^2/[c_p D^2]$; γ^* is introduced correspondingly by defining a hybridized length scale D^*. The most significant difference of DES and SAS methods is the different definition of D given by $D = d/f_w^{1/2}$ and $D = \ell_{vK,tot}$, respectively. Here, d is the distance to the wall, and the function f_w is defined in Ref. 49. The modified von Kármán length scale is given by $\ell_{vK,tot} = |S_{tot}/S'_{tot}|$, S'_{tot} being the derivative of S_{tot}.[17] Regarding the analysis of the ν_t transport equation, it is again beneficial to distinguish between analysis options $\mathcal{O}_1$ and $\mathcal{O}_2$, which include or neglect contributions due to $D\nu_t/Dt$. We neglect gradients of $\delta\nu_t/\nu_t$ in space and time, which corresponds to assumption $\mathcal{A}_2$, see the third paragraph. The variational analysis of the ν_t equation follows the analysis of $k-\epsilon$ and $k-\omega$ models. The RANS parameter γ is replaced by the unknown γ^*. We obtain minimal error models $\gamma_1^* = 1 + S_+^{-1}(\gamma - 1)$ and $\gamma_2^* = 1 + \ell_+^2(\gamma - 1)$ in options $\mathcal{O}_1$ and $\mathcal{O}_2$, respectively: $\ell_+ = \ell/\ell_{tot}$ and $S_+^{-1} = S^{-1}/S_{tot}^{-1}$ replace resolution indicators L_+ and τ_+ obtained for $k-\epsilon$ and $k-\omega$ models; that is, ν_t models replace characteristic length and time scales by ℓ and S^{-1}. The D_1^{*2}, D_2^{*2} expressions are obtained by combining the γ^* definition with the corresponding γ^* mode controls.

Regarding the minimal error methods presented above, a question of interest is about the comparison with standard LES. To prepare the discussion of this question in the next paragraph, we consider an identical rewriting of the modeled viscosity $\nu_t = C_\mu k^{1/2} L$ combined with the identically rewritten KES/KOS k equation in the $\mathcal{O}_2$ option involving the usual diffusion term

$$\frac{Dk}{Dt} = \frac{k^{3/2}}{L}\left(\frac{C_\mu L^2 S^2}{k} - 1\right) + D_k. \tag{2}$$

The relation of methods presented here to equilibrium LES can be seen based on the production–dissipation equilibrium $k = C_\mu L^2 S^2$ of Eq. (2). Combined with $\nu_t = C_\mu k^{1/2} L$, we obtain $\nu_t = c_S L^2 S$, where $c_S = C_\mu^{3/2}$ recovers the standard Smagorinsky constant $c_S = 0.164^2$ if $C_\mu = 0.09$ is used. The result $\nu_t = c_S L^2 S$ obtained requires an equation to provide L. The most appropriate way to address this question is the use of DES–SAS equations to directly provide ν_t. We note that the comparison of $\nu_t = c_S L^2 S$ with the definition $\nu_t = \ell^2 S$ implies $\ell^2 = c_S L^2$.

The comparison of equations presented in the preceding paragraph with LES shows that these equations are equivalent to standard equilibrium and k-equation-based LES, and the difference is that $L = \Delta$ is considered in standard LES (Δ being the filter width), whereas L is provided via the scale equation here. We note the following regarding the use of a fluctuating L and the non-fluctuating Δ. First, by invoking the usual PANS/PITM assumption $\epsilon = \epsilon_{tot}$ only here for illustration purposes, $L = k^{3/2}/\epsilon \approx k^{3/2}/\epsilon_{tot}$ needs to be calculated as a fluctuating variable according to its definition. Second, the approach presented here enables the calculation of an error-free fluctuating L, which does not apply to $L = \Delta$. In particular, the LES setting $L = \Delta$ does not ensure that the RANS-type k equation is minimally affected by fluctuations, the opposite may be the case: depending on the grid applied, the concept of independent settings of possibly large Δ may lead to a large production-to-dissipation ratio $C_\mu L^2 S^2/k$, which may significantly enhance the generation of fluctuations.

Table V compares Tables I–III minimal error results (which recover previous CES results) with usually applied methods by considering analysis option $\mathcal{O}_2$ for simplicity. The predominant feature of minimal error methods is that this approach does not only minimize the hybridization error, but it implements an error-free mode interplay. In hybrid simulations, there are two sorts of resolution information: there is the actual resolution seen in simulations (measured, e.g., by L_+), and there is resolution imposed on the simulation by the model [given, e.g., by providing in PANS approaches a desired R value in $\alpha_2^* = 1 + R(\alpha - 1)$]. In minimal error methods, the model receives information about the actual flow resolution via L_+, and it imposes a model-implied resolution equal to the actual flow resolution via $\alpha_2^* = 1 + L_+^2(\alpha - 1)$, see also the illustration in Fig. 1(a). Without this equality of actual and imposed resolution, there would be no reflection of actual resolution in the model. By contrast, a typical $\mathcal{E}_1$ error of other hybrid methods is that the model imposes a desired resolution independent of the actual flow resolution [see Fig. 1(b)]. The problem of this concept is that there is no mechanism to actually implement the imposed flow resolution. The latter has simple consequences: there is no way for the model to properly respond to changes of the flow resolution implied by grid/Re variations. Another typical ($\mathcal{E}_2$) error of other hybrid methods is the approximate mode interplay representation discussed below.

In particular, regarding the PANS–PITM comparison in Table V, we focus on KES/KOS models. We note that usually applied PANS and PITM approaches (R^{PANS} and R^{PITM}) do not represent minimal error approaches. The errors implied by these methods are different. In PANS, where an imposed R^{PANS} is used, we observe an $\mathcal{E}_1$ error: the interaction of resolved and modeled modes (which takes place via $R = L_+^2$ in CES methods) is dysfunctional because the model does not receive information about the resolved motion. In regard to PITM, an $\mathcal{E}_2$ error is observed: an inconsistent mode interaction R^{PITM} is applied in non-homogeneous flow simulations (and $\epsilon_+ = 1$ is assumed), see the discussion in Ref. 40. Similar observations can be made in regard to the comparison of minimal error DES–SAS methods with usually applied approaches in Table V. According to the model structure, this comparison is made at best by looking at implications for D_*/D. The DES approach and its variants reveal an $\mathcal{E}_1$ error, whereas the SAS approach reveals an $\mathcal{E}_2$ error ($[\ell_{vK}]_+$ represents an approximation to the minimal error result for D_*/D). As seen for PANS and PITM, it is of interest that DES and SAS, too, correspond to parametrizations of

TABLE V. Comparison of minimal error results with popular hybrid RANS–LES, LES, including their error types $\mathcal{E}_1$ and $\mathcal{E}_2$. We applied $\tilde{d} = \min(d, C_{DES}\Delta)$ (C_{DES} is a constant), $k_+^{mod} = (C_+\Delta/L_{tot})^{2/3}/[1 + (C_+\Delta/L_{tot})^3]^{2/9}$, and $\nu_t^{BL} = \nu_{t,tot} - \nu_{t,res}$.

Method	Minimal error (CES) methods	Usually applied methods	Implied error
PANS–PITM	KES: $\alpha_2^* = 1 + R(\alpha - 1)$: $R = L_+^2$ (KOS: $\alpha = \beta$)	$R^{\mathrm{PANS}} = R_{imp}$	$\mathcal{E}_1$
		$R^{\mathrm{PITM}} = k_+^{mod}$	$\mathcal{E}_2$
DES–SAS	$\gamma_2^* = \frac{c_d\ell^2}{c_p D_2^{*2}} : \frac{D_2^{*2}}{D} = \frac{\gamma^{1/2}\ell_+}{\gamma_2^{*1/2}} = \frac{\gamma^{1/2}\ell_+}{[1 + \ell_+^2(\gamma - 1)]^{1/2}}$	$D^{*\mathrm{DES}}/D = \tilde{d}\tilde{f}_w^{-1/2}/(df_w^{-1/2})$	$\mathcal{E}_1$
		$D^{*\mathrm{SAS}}/D = \ell_{vK}/\ell_{vK,tot}$	$\mathcal{E}_2$
ML	$\gamma_2^* = 1 + \ell_+^2(\gamma - 1)$	$1 - \gamma^* = \gamma_p^* - \gamma$, $\gamma_p^* = \gamma_p^{*\mathrm{ML}}$	$\mathcal{E}_1$
		NA	$\mathcal{E}_2$
k Eq.-LES	KES/KOS: $\nu_t = C_\mu k^{1/2}L$, $\frac{Dk}{Dt} = \nu_t S^2 - \frac{k^{3/2}}{L} + D_k$	$L^{\mathrm{LES}} = \Delta$	$\mathcal{E}_1$
		NA	$\mathcal{E}_2$
Equi. LES	$\nu_t = c_S L^2 S = \ell^2 S$	$\nu_t^{\mathrm{Equi-LES}} = c_S S\Delta^2$	$\mathcal{E}_1$
		$\nu_t^{\mathrm{WMLES}} = \nu_t^{\mathrm{BL}}$ and ν_t^{LES}	$\mathcal{E}_2$

ℓ_+^2, as may be seen by using the corresponding D_*/D expressions on the left-hand side (LHS) of $D_2^*/D = \gamma^{1/2}\ell_+/[1 + \ell_+^2(\gamma - 1)]^{1/2}$. Similar trends are seen in regard to ML supported model improvements. Only $\mathcal{E}_1$ error methods are reported so far: the production in a modeled viscosity equation is modified to enable a match with desired lift coefficient or skin-friction coefficient distributions. However, to date, consistent and broadly applicable data-driven improvements for separated flows have not been achieved.[44]

In regard to the comparison with k-equation LES in Table V, the LES setting implies $L = (\Delta/L_{tot})L_{tot}$; that is, L is represented as a fraction of L_{tot}. The latter implies an $\mathcal{E}_1$ error: a resolution requirement is imposed, and the model does not receive information about the actual resolution. According to the author's knowledge, $\mathcal{E}_2$ error type simulations were not reported so far. It is worth noting that there is a difference between not fully resolving and resolving methods. The correct functioning of partially resolving methods requires that the model imposes a resolution equal to the actual resolution (see the discussion above). This condition is less stringent for resolving LES as long as both imposed and actual resolutions effectively correspond to an almost resolving simulation. The problem is that the question of whether LES resolution requirements are satisfied usually represents a non-trivial problem, especially for very high Re flows.[50] In regard to equilibrium LES, the usual LES assumption $L = \Delta$ in $\nu_t = c_S L^2 S$ is shown in Table V. The price for using $\nu_t = c_S S\Delta^2$ is an implied $\mathcal{E}_1$ error: the model imposes a desired resolution independent of the actual flow resolution. The concept of WMLES makes an attempt to reflect such information via the inclusion of $\nu_t^{BL} = \nu_{t,tot} - \nu_{t,res}$. The latter is restricted to the boundary layer (BL) region, and there is the question of whether the uncontrolled difference between the imposed $\nu_{t,tot}$ and $\nu_{t,res}$ provides a meaningful representation of the interaction of resolved and modeled motions.

This analysis can be summarized as follows:

1. A new concept is presented: minimal error partially and fully resolving simulation methods (i.e., methods that minimize the hybridization error). This approach represents a variant of ML. In particular, the methods presented use sample data (resolved motion produced by the model) on the fly to optimize the simulation by adjusting the model to the actual flow resolution (see Fig. 1). The approach can be applied in an exact analysis option $\mathcal{O}_1$ or in a simplified option $\mathcal{O}_2$.
2. The ML-based results presented significantly extend previously introduced CES methods: the approach enables different

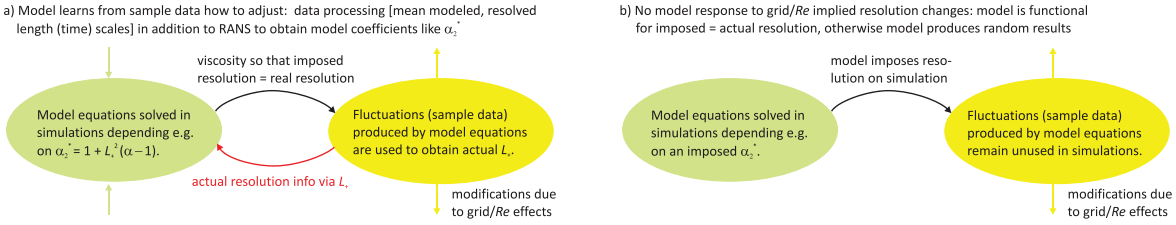

FIG. 1. An illustration of the interplay of model equations (which represent modeled motion) and fluctuations produced by model equations (which represent resolved motion, real turbulence): (a) minimal error CES simulations and (b) $\mathcal{E}_1$ errors of different hybrid RANS–LES and LES. Details of model equations are given in Tables I–III, and α_2^* (see Table I, option $\mathcal{O}_2$) is used here as an example for corresponding model parameters.

hybridizations (KES and KEK, KOS and KOK), and it can be applied to a variety of hybrid RANS–LES. In contrast to previous work, widely used DES and WMLES methods are now included. All the methods presented can be used as (L-driven depending on the formulation) LES in resolving mode having essential advantages to standard Δ-driven LES.

3. On this basis, it is shown that different hybrid RANS–LES models (PANS, PITM, DES, SAS, and WMLES) reveal $\mathcal{E}_1$ and $\mathcal{E}_2$ errors, there is either no reflection of the actual flow resolution (a desired flow resolution is imposed, but it cannot be realized because there is no mechanism for that), or the flow resolution is approximately involved without accuracy control. Standard LES suffer from typical $\mathcal{E}_1$ errors and the usual question of whether resolution requirements are met.[50]
4. The application of the minimal error methods reported here enables it to overcome these errors. Compared to RANS, the only difference is the need to implement, basically, the same mode interplay mechanism, which is relatively simple: it needs the calculation of mean modeled and resolved length or time scales (see Fig. 1). The approach presented also enables it to overcome other typical DES and WMLES problems (effect of grid design, grid matching, and model option settings).
5. We need reliable methods to simulate high Re flows. LES and experiments are restricted by resolution requirements, and hybrid RANS–LES are known to be unreliable. The difference between minimal error methods and other methods is that the model provides an error-free simulation contribution in response to the flow resolution (see Fig. 1). Without this ability, simulation methods cannot provide reliable predictions under conditions where validation data are unavailable.

ACKNOWLEDGMENTS

I would like to acknowledge support from the National Science Foundation [Atmospheric & Geospace Sciences (AGS), Grant No. 2137351, with Dr. N. Anderson as Technical Officer] and support from the Hanse-Wissenschaftskolleg (Delmenhorst, Germany, with Dr. M. Kastner as Technical Officer). This work was supported by Wyoming NASA Space Grant Consortium (NASA Grant No. 80NSSC20M0113) and the University of Wyoming School of Computing (Wyoming Innovation Partnership grant).

AUTHOR DECLARATIONS

Conflict of Interest

The author has no conflicts to disclose.

DATA AVAILABILITY

The data that support the findings of this study are available within the article.

APPENDIX: CALCULATION OF RESOLUTION INDICATORS

A relevant technical detail of minimal error methods is the calculation of L_+ (τ_+ is calculated correspondingly). The turbulence length scale resolution ratio $L_+ = L/L_{tot}$ involves modeled (L) and total contributions (L_{tot}).[37] The modeled contribution is calculated by $L = \langle k \rangle^{3/2}/\langle \epsilon \rangle$, where the brackets refer to averaging in time. The total length scale is calculated correspondingly by $L_{tot} = k_{tot}^{3/2}/\epsilon_{tot}$. Corresponding to $k_{tot} = \langle k \rangle + k_{res}$, ϵ_{tot} is the sum of modeled and resolved contributions, $\epsilon_{tot} = \langle \epsilon \rangle + \epsilon_{res}$. Here, the resolved contributions are calculated by $k_{res} = (\langle \tilde{U}_i \tilde{U}_i \rangle - \langle \tilde{U}_i \rangle \langle \tilde{U}_i \rangle)/2$, $\epsilon_{res} = \nu(\langle \partial \tilde{U}_i/\partial x_j \partial \tilde{U}_i/\partial x_j \rangle - \langle \partial \tilde{U}_i/\partial x_j \rangle \langle \partial \tilde{U}_i/\partial x_j \rangle)$.

REFERENCES

[1] S. B. Pope, *Turbulent Flows* (Cambridge University Press, Cambridge, 2000).
[2] S. Heinz, "A review of hybrid RANS–LES methods for turbulent flows: Concepts and applications," Prog. Aerosp. Sci. **114**, 100597 (2020).
[3] J. Fröhlich and D. V. Terzi, "Hybrid LES/RANS methods for the simulation of turbulent flows," Prog. Aerosp. Sci. **44**(5), 349–377 (2008).
[4] B. Chaouat, "The state of the art of hybrid RANS/LES modeling for the simulation of turbulent flows," Flow Turbul. Combust. **99**(2), 279–327 (2017).
[5] U. Piomelli, "Large eddy simulations in 2030 and beyond," Philos. Trans. R. Soc. A **372**(2022), 20130320 (2014).
[6] J. Larsson, S. Kawai, J. Bodart, and I. Bermejo-Moreno, "Large eddy simulation with modeled wall-stress: Recent progress and future directions," Mech. Eng. Rev. **3**(1), 15–00418 (2016).
[7] S. T. Bose and G. I. Park, "Wall-modeled large-eddy simulation for complex turbulent flows," Annu. Rev. Fluid Mech. **50**, 535–561 (2018).
[8] X. L. D. Huang, X. I. A. Yang, and R. F. Kunz, "Wall-modeled large-eddy simulations of spanwise rotating turbulent channels—Comparing a physics-based approach and a data-based approach," Phys. Fluids **31**(12), 125105 (2019).
[9] H. Hosseinzade and D. J. Bergstrom, "Time-averaging and temporal-filtering in wall-modeled large eddy simulation," Phys. Fluids **33**(3), 035108 (2021).
[10] R. Zangeneh, "Data-driven model for improving wall-modeled large-eddy simulation of supersonic turbulent flows with separation," Phys. Fluids **33**(12), 126103 (2021).
[11] S. Blanchard, N. Odier, L. Gicquel, B. Cuenot, and F. Nicoud, "Stochastic forcing for sub-grid scale models in wall-modeled large-eddy simulation," Phys. Fluids **33**(9), 095123 (2021).
[12] P. R. Spalart, W. H. Jou, M. Strelets, and S. R. Allmaras, "Comments on the feasibility of LES for wings, and on a hybrid RANS/LES approach," in *Advances in DNS/LES*, edited by C. Liu and Z. Liu (Greyden Press, Columbus, 1997), pp. 137–147.
[13] P. R. Spalart, "Detached-eddy simulation," Annu. Rev. Fluid Mech. **41**, 181–202 (2009).
[14] C. Friess, R. Manceau, and T. B. Gatski, "Toward an equivalence criterion for hybrid RANS/LES methods," Comput. Fluids **122**(11), 233–246 (2015).
[15] Y. Shi and W. Kollmann, "Improved delayed detached eddy simulation of a porous wavy trailing edge," Phys. Fluids **33**(5), 055128 (2021).
[16] F. Li, C. He, P. Wang, and Y. Liu, "Unsteady analysis of turbulent flow and heat transfer behind a wall-proximity square rib using dynamic delayed detached-eddy simulation," Phys. Fluids **33**(5), 055104 (2021).
[17] F. R. Menter and Y. Egorov, "The scale-adaptive simulation method for unsteady turbulent flow prediction: Part 1: Theory and model description," Flow Turbul. Combust. **78**(1), 113–138 (2010).
[18] S. Jakirlić and R. Maduta, "Extending the bounds of 'steady' RANS closures: Toward an instability-sensitive Reynolds stress model," Int. J. Heat Fluid Flow **51**(2), 175–194 (2015).
[19] J. Li, C. Zhong, D. Pan, and C. Zhuo, "A gas-kinetic scheme coupled with SST model for turbulent flows," Comput. Math. Appl. **78**(4), 1227–1242 (2019).
[20] S. Guo, Y. Feng, and P. Sagaut, "Improved standard thermal lattice Boltzmann model with hybrid recursive regularization for compressible laminar and turbulent flows," Phys. Fluids **32**(12), 126108 (2020).
[21] S. Wilhelm, J. Jacob, and P. Sagaut, "An explicit power-law-based wall model for lattice Boltzmann method–Reynolds-averaged numerical simulations of the flow around airfoils," Phys. Fluids **30**(6), 065111 (2018).
[22] S. Chen, Z. Xia, S. Pei, J. Wang, Y. Yang, Z. Xiao, and Y. Shi, "Reynolds-stress-constrained large-eddy simulation of wall-bounded turbulent flows," J. Fluid Mech. **703**, 1–28 (2012).
[23] S. Heinz, *Statistical Mechanics of Turbulent Flows* (Springer, Berlin, 2003).

[24]S. Heinz, "On Fokker–Planck equations for turbulent reacting flows. Part 2. Filter density function for large eddy simulation," Flow Turbul. Combust. **70**(1), 153–181 (2003).
[25]S. Heinz, "Unified turbulence models for LES and RANS, FDF and PDF simulations," Theor. Comput. Fluid Dyn. **21**(2), 99–118 (2007).
[26]S. Heinz, "Realizability of dynamic subgrid-scale stress models via stochastic analysis," Monte Carlo Methods Appl. **14**(4), 311–329 (2008).
[27]S. Heinz and H. Gopalan, "Realizable versus non-realizable dynamic subgrid-scale stress models," Phys. Fluids **24**(11), 115105 (2012).
[28]H. Gopalan, S. Heinz, and M. Stöllinger, "A unified RANS–LES model: Computational development, accuracy and cost," J. Comput. Phys. **249**, 249–279 (2013).
[29]R. Mokhtarpoor, S. Heinz, and M. Stoellinger, "Dynamic unified RANS–LES simulations of high Reynolds number separated flows," Phys. Fluids **28**(9), 095101 (2016).
[30]R. Mokhtarpoor and S. Heinz, "Dynamic large eddy simulation: Stability via realizability," Phys. Fluids **29**(10), 105104 (2017).
[31]M. Stöllinger, S. Heinz, C. Zemtsop, H. Gopalan, and R. Mokhtarpoor, "Stochastic-based RANS–LES simulations of swirling turbulent jet flows," Int. J. Nonlinear Sci. Numer. Simul. **18**(5), 351–369 (2017).
[32]S. S. Girimaji, "Partially-averaged Navier–Stokes method for turbulence: A Reynolds-averaged Navier–Stokes to direct numerical simulation bridging method," ASME J. Appl. Mech. **73**(3), 413–421 (2006).
[33]C. Kamble and S. S. Girimaji, "Characterization of coherent structures in turbulent wake of a sphere using partially averaged Navier–Stokes (PANS) simulations," Phys. Fluids **32**(10), 105110 (2020).
[34]T. S. Fowler, F. D. Witherden, and S. S. Girimaji, "Partially-averaged Navier–Stokes simulations of turbulent flow past a square cylinder: Comparative assessment of statistics and coherent structures at different resolutions," Phys. Fluids **32**(12), 125106 (2020).
[35]B. Chaouat and R. Schiestel, "A new partially integrated transport model for subgrid-scale stresses and dissipation rate for turbulent developing flows," Phys. Fluids **17**(6), 065106 (2005).
[36]B. Chaouat and R. Schiestel, "Analytical insights into the partially integrated transport modeling method for hybrid Reynolds averaged Navier–Stokes equations-large eddy simulations of turbulent flows," Phys. Fluids **24**(8), 085106 (2012).
[37]S. Heinz, "The large eddy simulation capability of Reynolds-averaged Navier–Stokes equations: Analytical results," Phys. Fluids **31**(2), 021702 (2019).
[38]S. Heinz, R. Mokhtarpoor, and M. Stoellinger, "Theory-based Reynolds-averaged Navier–Stokes equations with large eddy simulation capability for separated turbulent flow simulations," Phys. Fluids **32**(6), 065102 (2020).
[39]S. Heinz, "The continuous eddy simulation capability of velocity and scalar probability density function equations for turbulent flows," Phys. Fluids **33**(2), 025107 (2021).
[40]S. Heinz, "Remarks on energy partitioning control in the PITM hybrid RANS/LES method for the simulation of turbulent flows," Flow Turbul. Combust. **108**(4), 927–933 (2022).
[41]S. Heinz, "Theory-based mesoscale to microscale coupling for wind energy applications," Appl. Math. Modell. **98**, 563–575 (2021).
[42]S. Heinz, J. Peinke, and B. Stoevesandt, "Cutting-edge turbulence simulation methods for wind energy and aerospace problems," Fluids **6**, 288 (2021).
[43]A. Fagbade and S. Heinz, "Application of mode-controlled hybrid RANS–LES to the NASA wall-mounted hump flow," AIAA Paper No. 22-0180, 2022.
[44]C. L. Rumsey, G. N. Coleman, and L. Wang, "In search of data-driven improvements to RANS models applied to separated flows," AIAA Paper No. 22-0937, 2022.
[45]S. W. Haering, T. A. Oliver, and R. D. Moser, "Active model split hybrid RANS/LES," Phys. Rev. Fluids **7**(1), 014603 (2022).
[46]E. Plaut and S. Heinz, "Exact eddy-viscosity equation for turbulent wall flows—Implications for computational fluid dynamics models," AIAA J. **60**(3), 1347–1364 (2022).
[47]S. Heinz, "On mean flow universality of turbulent wall flows. I. High Reynolds number flow analysis," J. Turbul. **19**(11–12), 929–958 (2018).
[48]S. Heinz, "On mean flow universality of turbulent wall flows. II. Asymptotic flow analysis," J. Turbul. **20**(2), 174–193 (2019).
[49]P. R. Spalart and S. R. Allmaras, "A one-equation turbulence model for aerodynamic flows," Rech. Aérosp. **1**, 5–21 (1994).
[50]L. Davidson, "Large eddy simulations: How to evaluate resolution," Int. J. Heat Fluid Flow **30**(5), 1016–1025 (2009).